Frontiers of Information Technology & Electronic Engineering
www.jzus.zju.edu.cn; engineering.cae.cn; www.springerlink.com
ISSN 2095-9184 (print); ISSN 2095-9230 (online)
E-mail: jzus@zju.edu.cn

A height estimation method based on a beamspace joint alternating iterative algorithm in MIMO radar*

Derui TANG, Yongbo ZHAO†‡, Shuaijie ZHANG

National Key Laboratory of Radar Signal Processing, Xidian University, Xi'an 710071, China

†E-mail: ybzhao@xidian.edu.cn

Received Jan. 13, 2025; Revision accepted June 10, 2025; Crosschecked Aug. 28, 2025

Abstract: This paper discusses the problem of low-elevation target height estimation for multiple-input multiple-output (MIMO) radar in multipath environments. The beamspace compresses the data and is ideal for reducing the computational burden of elevation estimation. To obtain the height parameter of the target accurately, we propose a height estimation method based on a beamspace joint alternating iterative (BJAI) algorithm in MIMO radar. This method mainly converts the reduced-dimensional MIMO radar element space data into beamspace data and whitens them to improve the reliability. Then, a simplified model is used to obtain the initial value of the elevation, and we combine the reflection coefficient and the target elevation angle for alternate estimation. Finally, we calculate the target height using the obtained elevation information. Simulation results verify that the proposed algorithm has high estimation accuracy and strong robustness.

Key words: Multipath environment; Multiple-input multiple-output (MIMO) radar height estimation; Beamspace processing and whitening; Joint alternating iterative

https://doi.org/10.1631/FITEE.2500030 **CLC number:** TN95

1 Introduction

Meter-wave radar, also known as ultrashort wave or very high frequency (VHF) radar, generally refers to radar operating in the meter-wave band (Gage and Green, 1978; Zheng et al., 2023). Because of its long wavelength and wide beam width, meter-wave radar has a strong ground reflection echo when measuring targets at low elevations. The direct signal of the reflected target and the coherent multipath signal reflected along the ground enter the main beam of the radar together (Zhu et al., 2017; Tan and Nie, 2018). The direct signal and multipath signal are usually difficult to separate in the time, Doppler, and spatial domains. These problems seriously affect the accuracy of the estimated elevation, and it is unrealistic to improve the elevation estimation accuracy simply by increasing the physical aperture of the array. As a new radar system, multiple-input multiple-output (MIMO) radar (Li and Stoica, 2007; Zhang et al., 2012; Shi et al., 2021) has virtual aperture expansion characteristics and obvious advantages over traditional radar in terms of anti-interference, anti-clutter, low interception, and angular resolution (Zhou et al., 2016). Therefore, it is more appropriate to use MIMO radar to handle target height estimation in a multipath environment, but how to find an accurate and robust method is an urgent problem that needs to be solved.

In recent years, there has been rapid development of array signal processing, leading to the emergence

‡ Corresponding author

* Project supported by the National Natural Science Foundation of China (No. 62271379), the National Radar Signal Processing Laboratory (No. KGJ202401), and the Fundamental Research Funds for the Central Universities and the Innovation Fund of Xidian University (No. YJSJ24011)

ORCID: Derui TANG, https://orcid.org/0009-0002-1071-5301; Yongbo ZHAO, https://orcid.org/0000-0002-6453-0786

of many super-resolution methods (Carlin et al., 2013; Yang et al., 2020; Zheng et al., 2022). These methods can be broadly categorized into subspace algorithms and maximum likelihood (ML) algorithms. Subspace algorithms, such as MUSIC (Yin and Zhang, 2020) and ESPRIT (Feng et al., 2021), are commonly used. However, they require decoherence processing (Shi et al., 2016) to be completed first when estimating the target elevation angle, as they cannot directly process coherent signals. On the other hand, ML (Ziskind and Wax, 1988) algorithms can directly process coherent signals and are widely used in height estimation problems. The angle and reflection surface height joint estimation (ARJE) algorithm (Wang SH et al., 2016) is a method based on eigenvalue decomposition for complex terrains. It offers enhanced robustness by searching for more parameters. Beamspace (Xu and Zhao, 2019) reduces the data transmission volume, storage, and calculation, but sacrifices some degrees of freedom. To reduce the computational burden, the beamspace improved maximum likelihood (BIML) algorithm (Liu J et al., 2010) for MIMO radar was proposed for elevation estimation. The BIML algorithm uses prior knowledge of geometric information to reduce search dimensions and beamspace processing to reduce data dimensions. The three-dimensional beamspace maximum likelihood data fusion (3D-BMLF) algorithm (Chen S et al., 2022) converts element space data into beamspace data and uses eigenvectors to find closed-form solutions. The calculation amount is low, but the accuracy is subject to certain limitations. In addition, the refined maximum likelihood (RML) estimation method (Lo and Litva, 1991) takes advantage of prior information, such as radar height, target range, location of the multipath reflection point, multipath reflection coefficient, and multipath mirror geometry. Although the prior information contributes to the good performance of ML methods, these methods are usually applicable only to ideal smooth reflecting surfaces. In practice, it is difficult to obtain the relevant parameters.

In response to the above problems and research methods, we propose a height estimation method based on a beamspace joint alternating iterative (BJAI) algorithm in MIMO radar. This algorithm does not require prior information about the spatial distribution of the multipath. It first uses a simplified model in a multipath environment to obtain an initial estimation of the elevation of the target and performs reduced-dimensional processing on the MIMO radar. Then, based on the initial elevation estimation (Tang et al., 2024), the element space data are converted into the beamspace data and whitened. Finally, the reflection coefficient and the target elevation angle are combined for alternating iterative estimation, which ensures effective estimation accuracy while reducing the computational complexity of the algorithm. Simulation results show that this algorithm has strong robustness and high estimation accuracy.

The main contributions of this paper are as follows:

1. A new method of height estimation based on a BJAI algorithm in MIMO radar is proposed. This method does not require any prior information about terrain and reflection paths and enhances the robustness of the multipath propagation model in complex terrains.

2. Addressing the challenge of MIMO radar target height estimation in complex terrains involves initially using dimensionality reduction transformation and beamspace processing. Subsequently, the issue is resolved by alternately and iteratively estimating the reflection coefficient and target elevation angle. The multivariable optimization problem is decomposed into multiple single-variable optimization subproblems.

3. Simulation analysis and real data results show that the proposed algorithm has strong robustness and high estimation accuracy in complex terrains.

2 Multipath signal model

We consider a narrowband configured monostatic MIMO radar consisting of a uniform linear array. The radar is assumed to use a pulsed system with a transceiver co-located antenna design and evenly distributed vertically, and the detection targets are mostly far-field targets, which can easily meet the Rayleigh conditions on smooth ground. The geometry of the target height estimation scenario for monostatic MIMO radar in the low-elevation area is shown in Fig. 1. In the MIMO radar system, there are M transmitting sensors and receiving sensors. The height of the antenna center is h_a. The element spacing of the antenna is denoted by d, which is less than or equal to $\lambda/2$. λ is the

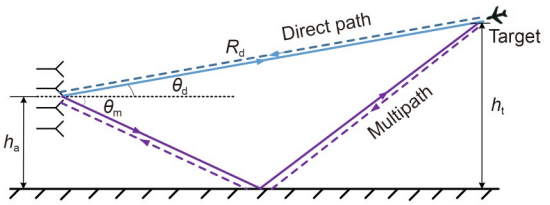

Fig. 1 Geometry of the target height estimation scenario for monostatic MIMO radar in the low-elevation area

wavelength, and the target-antenna element distance is R_d. In practical applications, both receiving and transmitting two-way multipath signals should be taken into consideration, so the echo signals received by the antenna elements should come from four different paths. The monostatic MIMO radar transmitter emits a set of mutually orthogonal signals.

After matched filtering, the received signal can be written as (Wang XP et al., 2015)

$$\boldsymbol{X}(t)=\boldsymbol{B}_{tr}s(t)+\boldsymbol{n}(t), \tag{1}$$

where $\boldsymbol{B}_{tr}=\boldsymbol{b}_r(\theta_d,\theta_m)\otimes\boldsymbol{b}_t(\theta_d,\theta_m)\in\mathbb{C}^{M^2\times 1}$, and $\otimes$ represents the Kronecker product. $s(t)$ is the complex envelope of the transmitted signal. The composite transmitter and receiver steering vectors are denoted by $\boldsymbol{b}_t(\theta_d,\theta_m)\in\mathbb{C}^{M\times 1}$ and $\boldsymbol{b}_r(\theta_d,\theta_m)\in\mathbb{C}^{M\times 1}$, respectively. Here, θ_d and θ_m represent the arrival angles of the direct signal and multipath signal, respectively, and $\boldsymbol{n}(t)\in\mathbb{C}^{M^2\times 1}$ is zero-mean Gaussian white noise, which is uncorrelated with the target signal.

The composite steering vectors include direct and multipath signals, which are shown as

$$\boldsymbol{b}_t(\theta_d,\theta_m)=\boldsymbol{a}_t(\theta_d)+\rho e^{-j2\pi\Delta R/\lambda}\boldsymbol{a}_t(\theta_m), \tag{2}$$
$$\boldsymbol{b}_r(\theta_d,\theta_m)=\boldsymbol{a}_r(\theta_d)+\rho e^{-j2\pi\Delta R/\lambda}\boldsymbol{a}_r(\theta_m), \tag{3}$$

where

$$\boldsymbol{a}_t(\theta)=\left[1, e^{-j2\pi d\sin\theta/\lambda},\cdots, e^{-j2\pi(M-1)d\sin\theta/\lambda}\right]^T, \tag{4}$$
$$\boldsymbol{a}_r(\theta)=\left[1, e^{-j2\pi d\sin\theta/\lambda},\cdots, e^{-j2\pi(M-1)d\sin\theta/\lambda}\right]^T. \tag{5}$$

Here, $\boldsymbol{a}_t(\theta)$ and $\boldsymbol{a}_r(\theta)$ are the transmitter steering vector and receiver steering vector, respectively. $\Delta R=2h_a(\sin\theta_d+h_a/R_d)$ is the path-difference between the direct and multipath signals, j denotes the imaginary unit, and ρ is the surface reflection coefficient (Lo and Litva, 1991).

Assuming that the number of snapshots of the received data is L, the observation data matrix can be written as

$$\boldsymbol{X}=\boldsymbol{B}_{tr}\boldsymbol{S}+\boldsymbol{N}, \tag{6}$$

where $\boldsymbol{X}=[x(t_1),x(t_2),\cdots,x(t_L)]\in\mathbb{C}^{M^2\times L}$, $\boldsymbol{S}=[s(t_1),s(t_2),\cdots,s(t_L)]\in\mathbb{C}^{1\times L}$, and $\boldsymbol{N}=[\boldsymbol{n}(t_1),\boldsymbol{n}(t_2),\cdots,\boldsymbol{n}(t_L)]\in\mathbb{C}^{M^2\times L}$.

3 BJAI algorithm for height estimation

In this section, we present the proposed BJAI algorithm, which is appropriate for target height estimation in a MIMO radar setup. The BJAI algorithm first uses a simplified model to roughly estimate the target elevation angle and then reduces the dimension of the received signal based on reduced-dimensional transformation and beamspace processing. After that, the BJAI algorithm estimates the target height using the JAI algorithm (Liu Y et al., 2018).

3.1 Initial angle estimation on a simplified model

According to the MIMO radar multipath signal reflection model and the geometric relationship of the low-elevation area, the elevation expression of the reflection path can be obtained as

$$\theta_m=-\arcsin(\sin\theta_d+2h_a/R_d). \tag{7}$$

In general, $R_d\gg h_a$; thus, taking the receiver as an example, combined with the steering vector, we can obtain (Chen C et al., 2022)

$$\boldsymbol{a}_r(\theta_m)\approx\boldsymbol{a}_r(-\theta_d)=\mathbf{TF}(\theta_d)\boldsymbol{a}_r(\theta_d), \tag{8}$$

where $\mathbf{TF}(\theta_d)$ is a diagonal matrix, whose expression is

$$\mathbf{TF}(\theta_d)=\mathrm{diag}\left(1, e^{j4\pi d\sin\theta_d/\lambda},\cdots, e^{j4\pi(M-1)d\sin\theta_d/\lambda}\right). \tag{9}$$

From the equations above, the composite receiver steering vector can be expressed as

$$\boldsymbol{b}_r(\theta_d,\theta_m)=\left[\boldsymbol{I}_M+\gamma\cdot\mathbf{TF}(\theta_d)\right]\boldsymbol{a}_r(\theta_d), \tag{10}$$

where $\gamma=\rho e^{-j2\pi\Delta R/\lambda}$ and $\boldsymbol{I}_M$ is an $M\times M$ identity matrix.

$\boldsymbol{b}_{\mathrm{r}}(\theta_{\mathrm{d}}, \theta_{\mathrm{m}})$ is a function of θ_{d}. Digital beamforming (DBF) scanning is performed on the received element-space data to obtain an initial elevation estimate $\hat{\theta}_{\mathrm{d}}^{(0)}$. In addition, $\hat{\theta}_{\mathrm{d}}^{(0)}$ can be used as the initial iteration of the algorithm and to determine the angle search range.

3.2 Reduced-dimensional transformation

In each column of the steering matrix $\boldsymbol{B}_{\mathrm{tr}}$ in MIMO radar, (M+M−1) elements are unique. Exploiting this feature, a reduced-dimensional transformation is adopted to lower the dimension of the received data $\boldsymbol{X}$ (Liu J et al., 2017):

$$\boldsymbol{C}(\theta_{\mathrm{d}}, \theta_{\mathrm{m}})=\boldsymbol{C}(\theta_{\mathrm{d}})+\rho \mathrm{e}^{-\mathrm{j}2\pi\Delta R/\lambda}\boldsymbol{C}(\theta_{\mathrm{m}}), \tag{11}$$

where $\boldsymbol{C}(\theta_{\mathrm{d}}, \theta_{\mathrm{m}})\in\mathbb{C}^{(M+M-1)\times 1}$ is the virtual composite steering vector and

$$\boldsymbol{C}(\theta)=\left[1, \mathrm{e}^{-\mathrm{j}2\pi d\sin\theta/\lambda}, \cdots, \mathrm{e}^{-\mathrm{j}2\pi(M+M-2)d\sin\theta/\lambda}\right]^{\mathrm{T}}. \tag{12}$$

$\boldsymbol{J}$ is a transformation matrix and can be expressed as

$$\boldsymbol{J}=\left[\boldsymbol{\Xi}_0^{\mathrm{T}}, \boldsymbol{\Xi}_1^{\mathrm{T}}, \cdots, \boldsymbol{\Xi}_{M-1}^{\mathrm{T}}\right]^{\mathrm{T}}, \tag{13}$$

where $\boldsymbol{\Xi}_m=\left[\boldsymbol{0}_{M\times m}, \boldsymbol{I}_M, \boldsymbol{0}_{M\times(M-m-1)}\right]\in\mathbb{C}^{M\times(M+M-1)}$ for m= 0, 1, ⋯, M − 1. Therefore, we can obtain

$$\boldsymbol{B}_{\mathrm{tr}}=\boldsymbol{J}\cdot\boldsymbol{C}(\theta_{\mathrm{d}}, \theta_{\mathrm{m}}). \tag{14}$$

According to the above relationship, a reduced-dimensional matrix can be defined as

$$\boldsymbol{T}=\boldsymbol{P}^{-1}\boldsymbol{J}^{\mathrm{H}}, \tag{15}$$

where $\boldsymbol{T}\in\mathbb{C}^{(M+M-1)\times M^2}$, and $[\cdot]^{\mathrm{H}}$ denotes the conjugate-transpose operator. $\boldsymbol{P}=(\boldsymbol{J}^{\mathrm{H}}\boldsymbol{J})^{1/2}$ is a diagonal matrix directly calculated as

$$\boldsymbol{P}=\mathrm{diag}\left[1, \sqrt{2}, \cdots, \sqrt{M}, \cdots, \sqrt{2}, 1\right]. \tag{16}$$

Consequently, using the reduced-dimensional transformation of the data matrix, $\boldsymbol{X}$ is implemented as follows:

$$\overline{\boldsymbol{X}}=\boldsymbol{T}(\boldsymbol{B}_{\mathrm{tr}}\boldsymbol{S}+\boldsymbol{N})=\boldsymbol{P}\cdot\boldsymbol{C}(\theta_{\mathrm{d}}, \theta_{\mathrm{m}})\cdot\boldsymbol{S}+\overline{\boldsymbol{N}}, \tag{17}$$

where $\overline{\boldsymbol{X}}\in\mathbb{C}^{(M+M-1)\times L}$ and $\overline{\boldsymbol{N}}\in\mathbb{C}^{(M+M-1)\times L}$ are the newly received data matrix and noise matrix, respectively. The reduced-dimensional data $\overline{\boldsymbol{X}}$ are equivalent to the received data of a virtual array of (M+M−1) array elements.

3.3 Beamspace multipath signals and data whitening

In Section 3.1, based on the DBF scanning of the array space data, a rough estimate of the arrival angle of the direct signal, $\hat{\theta}_{\mathrm{d}}^{(0)}$, can be obtained. A rough estimate of the arrival angle of the multipath signal is $-\hat{\theta}_{\mathrm{d}}^{(0)}$.

Based on the multipath signal propagation model, we define a beamspace conversion matrix $\boldsymbol{T}_{\mathrm{B}}$ of size (M+M−1)×3, which aims to convert the array element space data into the beamspace data:

$$\boldsymbol{T}_{\mathrm{B}}=\left[\boldsymbol{c}\left(\hat{\theta}_{\mathrm{d}}^{(0)}\right), \boldsymbol{c}(0), \boldsymbol{c}\left(-\hat{\theta}_{\mathrm{d}}^{(0)}\right)\right]. \tag{18}$$

The target data in the beamspace can be expressed as

$$\boldsymbol{X}_{\mathrm{B}}=\boldsymbol{T}_{\mathrm{B}}^{\mathrm{H}}\overline{\boldsymbol{X}}=\boldsymbol{T}_{\mathrm{B}}^{\mathrm{H}}\boldsymbol{P}\cdot\boldsymbol{C}(\theta_{\mathrm{d}}, \theta_{\mathrm{m}})\cdot\boldsymbol{S}+\boldsymbol{T}_{\mathrm{B}}^{\mathrm{H}}\overline{\boldsymbol{N}}, \tag{19}$$

where $\boldsymbol{X}_{\mathrm{B}}\in\mathbb{C}^{3\times L}$. The three rows of the beamspace data $\boldsymbol{X}_{\mathrm{B}}$ are the outputs of the beam forming in the three directions $\hat{\theta}_{\mathrm{d}}^{(0)}$, 0, and $-\hat{\theta}_{\mathrm{d}}^{(0)}$.

To keep the noise of the beamspace data as Gaussian white noise, it should be whitened. We combine the beamspace conversion matrix $\boldsymbol{T}_{\mathrm{B}}$ with whitening to obtain a new beamspace conversion matrix:

$$\boldsymbol{T}_{\mathrm{WB}}=\left(\boldsymbol{T}_{\mathrm{B}}^{\mathrm{H}}\boldsymbol{T}_{\mathrm{B}}\right)^{-1/2}\boldsymbol{T}_{\mathrm{B}}^{\mathrm{H}}, \tag{20}$$

where $\boldsymbol{T}_{\mathrm{WB}}\boldsymbol{T}_{\mathrm{WB}}^{\mathrm{H}}=\boldsymbol{I}_3$. Then, the whitened beamspace data can be expressed as

$$\boldsymbol{X}_{\mathrm{WB}}=\boldsymbol{T}_{\mathrm{WB}}\overline{\boldsymbol{X}}=\boldsymbol{T}_{\mathrm{WB}}\boldsymbol{P}\cdot\boldsymbol{C}(\theta_{\mathrm{d}}, \theta_{\mathrm{m}})\cdot\boldsymbol{S}+\boldsymbol{T}_{\mathrm{WB}}\overline{\boldsymbol{N}}, \tag{21}$$

where $\boldsymbol{X}_{\mathrm{WB}}\in\mathbb{C}^{3\times L}$. The noise of the whitened beamspace data is Gaussian white noise, which is uncorrelated. At present, most beamspace angle estimation or height estimation algorithms convert only array element space data into beamspace data and do not consider whether the noise after conversion is still Gaussian white noise, so they are not optimal.

The angle search interval selected here is

$$\theta\in\left(\hat{\theta}_{\mathrm{d}}^{(0)}-\theta_{3\mathrm{dB}}/2,\hat{\theta}_{\mathrm{d}}^{(0)}+\theta_{3\mathrm{dB}}/2\right),\tag{22}$$

where we define $\theta_{3\mathrm{dB}}=\dfrac{50.8\lambda}{(M+M-1)d}$ as the 3 dB beam width.

3.4 Joint alternating iterative estimation

The purpose of low-elevation estimation is to obtain the target elevation angle θ_{d} from the beamspace data $\boldsymbol{X}_{\mathrm{WB}}$. First, the covariance matrix of the beamspace can be estimated as

$$\hat{\boldsymbol{R}}_{\mathrm{WB}}(\bar{\rho},\theta_{\mathrm{d}})=\boldsymbol{X}_{\mathrm{WB}}(\bar{\rho},\theta_{\mathrm{d}})\cdot\boldsymbol{X}_{\mathrm{WB}}^{\mathrm{H}}(\bar{\rho},\theta_{\mathrm{d}})/L,\tag{23}$$

where $\hat{\boldsymbol{R}}_{\mathrm{WB}}\in\mathbb{C}^{3\times3}$, $\bar{\rho}=\rho\mathrm{e}^{-\mathrm{j}2\pi\Delta R/\lambda}$.

For the symmetrical direct and reflected signals, to improve the angle estimation accuracy, $\hat{\boldsymbol{R}}_{\mathrm{WB}}$ can be replaced by (Zoltowski and Lee, 1991)

$$\boldsymbol{R}_{\mathrm{WB}}=\frac{1}{2}\left(\hat{\boldsymbol{R}}_{\mathrm{WB}}+\hat{\boldsymbol{I}}_3\hat{\boldsymbol{R}}_{\mathrm{WB}}\hat{\boldsymbol{I}}_3\right),\tag{24}$$

where

$$\hat{\boldsymbol{I}}_3=\begin{bmatrix}0&0&1\\0&1&0\\1&0&0\end{bmatrix}.\tag{25}$$

The proposed algorithm involves the JAI estimation of $\bar{\rho}$ and θ_{d}. Subsequently, by performing singular value decomposition (SVD) on the covariance matrix $\boldsymbol{R}_{\mathrm{WB}}$, we can obtain

$$\boldsymbol{R}_{\mathrm{WB}}=\boldsymbol{E}_{\mathrm{s}}\boldsymbol{\Lambda}_{\mathrm{s}}\boldsymbol{E}_{\mathrm{s}}^{\mathrm{H}}+\boldsymbol{E}_{\mathrm{n}}\boldsymbol{\Lambda}_{\mathrm{n}}\boldsymbol{E}_{\mathrm{n}}^{\mathrm{H}},\tag{26}$$

where $\boldsymbol{E}_{\mathrm{s}}$ and $\boldsymbol{E}_{\mathrm{n}}$ constitute the signal subspace and noise subspace, respectively, and $\boldsymbol{\Lambda}_{\mathrm{s}}$ and $\boldsymbol{\Lambda}_{\mathrm{n}}$ represent two diagonal matrices whose diagonal elements correspond to the signal subspace eigenvalues and noise subspace eigenvalues, respectively.

Based on the arrival angle of the direct signal $\hat{\theta}_{\mathrm{d}}^{(0)}$ obtained in Section 3.1, the arrival angle of the multipath signal can be calculated from Eq. (7). At this point, only the reflection coefficient $\bar{\rho}$ is unknown. By solving the corresponding optimization problem, we can obtain $\hat{\bar{\rho}}^{(k+1)}$.

Claim 1 The closed-form solution for $\hat{\bar{\rho}}^{(k+1)}$ can be calculated using the Lagrange multipliers:

$$\boldsymbol{\xi}^{(k+1)}=\frac{\left[\boldsymbol{Q}^{\mathrm{H}}\boldsymbol{P}^{\mathrm{H}}\boldsymbol{T}_{\mathrm{WB}}^{\mathrm{H}}\boldsymbol{E}_{\mathrm{n}}\boldsymbol{E}_{\mathrm{n}}^{\mathrm{H}}\boldsymbol{T}_{\mathrm{WB}}\boldsymbol{P}\boldsymbol{Q}\right]^{-1}\boldsymbol{\omega}}{\boldsymbol{\omega}^{\mathrm{H}}\left[\boldsymbol{Q}^{\mathrm{H}}\boldsymbol{P}^{\mathrm{H}}\boldsymbol{T}_{\mathrm{WB}}^{\mathrm{H}}\boldsymbol{E}_{\mathrm{n}}\boldsymbol{E}_{\mathrm{n}}^{\mathrm{H}}\boldsymbol{T}_{\mathrm{WB}}\boldsymbol{P}\boldsymbol{Q}\right]^{-1}\boldsymbol{\omega}},\tag{27}$$

where $\boldsymbol{\xi}^{(k+1)}=\left[1,\hat{\bar{\rho}}^{(k+1)}\right]^{\mathrm{T}}$, $\boldsymbol{Q}=\left[\boldsymbol{c}(\theta_{\mathrm{d}}),\boldsymbol{c}(\theta_{\mathrm{m}})\right]$, and $\boldsymbol{\omega}=\left[1,0\right]^{\mathrm{T}}$. See the appendix for the proof.

Then, the above estimated parameter $\hat{\bar{\rho}}^{(k+1)}$ is used to solve the following optimization problem, thereby obtaining the parameter $\hat{\theta}_{\mathrm{d}}^{(k+1)}$ to estimate the target elevation angle. The optimization problem can be expressed as

$$\hat{\theta}_{\mathrm{d}}^{(k+1)}=\arg\max_{\theta_{\mathrm{d}}}\frac{\left\|\boldsymbol{T}_{\mathrm{WB}}\boldsymbol{P}\cdot\boldsymbol{C}(\hat{\bar{\rho}}^{(k+1)})\right\|_2^2}{F_{\mathrm{capon}}F_{\mathrm{music}}},\tag{28}$$

where $F_{\mathrm{capon}}=\boldsymbol{C}^{\mathrm{H}}(\hat{\bar{\rho}}^{(k+1)})\boldsymbol{P}^{\mathrm{H}}\boldsymbol{T}_{\mathrm{WB}}^{\mathrm{H}}\boldsymbol{R}_{\mathrm{WB}}^{-1}\boldsymbol{T}_{\mathrm{WB}}\boldsymbol{P}\cdot\boldsymbol{C}(\hat{\bar{\rho}}^{(k+1)})$, $F_{\mathrm{music}}=\boldsymbol{C}^{\mathrm{H}}(\hat{\bar{\rho}}^{(k+1)})\boldsymbol{P}^{\mathrm{H}}\boldsymbol{T}_{\mathrm{WB}}^{\mathrm{H}}\boldsymbol{E}_{\mathrm{n}}\boldsymbol{E}_{\mathrm{n}}^{\mathrm{H}}\boldsymbol{T}_{\mathrm{WB}}\boldsymbol{P}\cdot\boldsymbol{C}(\hat{\bar{\rho}}^{(k+1)})$, and $\|\cdot\|_2$ denotes the L2-norm. The Capon-based cost function needs to calculate the inverse operation of the matrix, but the covariance matrix of the beamspace is a third-order matrix, so the inverse operation does not involve a large amount of calculation.

The optimization problem combines the cost functions of Capon and music, which reduces the beam width of the scanning curve, enhances the sparsity of the signal, improves the estimation accuracy of the target elevation angle, and makes the algorithm more robust. At this point, we complete the optimization update in the $(k+1)^{\mathrm{th}}$ iteration and obtain the updated parameter vector $\left(\hat{\bar{\rho}}^{(k+1)},\hat{\theta}_{\mathrm{d}}^{(k+1)}\right)$. Using that vector, we repeat the abovementioned optimization iterative process to complete the next iterative update of the parameter vector until the algorithm converges.

The convergence condition of the proposed algorithm can be defined as follows: when the parameter estimates obtained in two adjacent iterations have not changed significantly and when $\left|\hat{\theta}_{\mathrm{d}}^{(k+1)}-\hat{\theta}_{\mathrm{d}}^{(k)}\right|/\hat{\theta}_{\mathrm{d}}^{(k)}\le\varepsilon$, the algorithm stops the iterative process, where ε is the given convergence threshold. In addition, the maximum number of iterations K of the algorithm can be given. When the number of iterations k is greater than K, the algorithm iterations are terminated.

Finally, when the algorithm meets the convergence conditions, we can obtain the estimated value of the target elevation angle $\hat{\theta}_{\mathrm{d}}$. The height information of the target can be calculated using the target elevation angle and the structural relationship between the target and the radar. For a target in the near distance, its height can be calculated as

$$\hat{H}_{\mathrm{t}}=h_{\mathrm{a}}+R_{\mathrm{d}}\sin\hat{\theta}_{\mathrm{d}}, \tag{29}$$

where $\hat{H}_{\mathrm{t}}$ denotes the height of the target. For a long-range target, the spherical earth model must be considered, and the target height based on the beamspace data can be subsequently obtained by

$$\hat{H}_{\mathrm{t}}\simeq h_{\mathrm{a}}+R_{\mathrm{d}}\sin\hat{\theta}_{\mathrm{d}}+\frac{R_{\mathrm{d}}^2}{2R_{\mathrm{e}}}, \tag{30}$$

where R_{e} is the effective radius of the earth. Therefore, we iterate the estimation process to obtain the final estimate. The estimation steps of the proposed algorithm for beamspace data are summarized in Algorithm 1.

Algorithm 1 Proposed algorithm

Step 1: Set the maximum number of iterations K, the number of iterations $k=0$, and the given convergence threshold ε.

Step 2: Obtain the initial angle estimate $\hat{\theta}_{\mathrm{d}}^{(0)}$ by DBF scanning in the simplified model.

Step 3: Use reduced-dimensional matrices to process data by Eq. (17).

Step 4: Obtain whitened beamspace data of $\boldsymbol{X}_{\mathrm{WB}}$ by Eq. (21), and obtain the angle search interval.

Step 5: Estimate the reflection coefficient $\hat{\rho}^{(k+1)}$ by Eq. (27), and update the parameters.

Step 6: Estimate the target elevation angle $\hat{\theta}_{\mathrm{d}}^{(k+1)}$ by Eq. (28), and update the parameters.

Step 7: If the maximum number of iterations or the convergence condition is satisfied, stop the iteration. Otherwise, set $k=k+1$ and go to Step 5.

Step 8: Calculate the target height $\hat{H}_{\mathrm{t}}$ by Eq. (29) or (30).

4 Simulation analysis and real data validation

4.1 Simulation analysis

In this subsection, because different reflective terrains exist, several simulations are presented to compare the performance of the proposed method in different scenarios. In the following simulations, a vertically uniformly distributed narrowband monostatic MIMO radar array is considered. The radar emits orthogonal waveform signals, and the number of sampling points in the pulse is 400. The noise type is zero-mean Gaussian white noise. We set $d=\lambda/2=0.5$ m, $L=64$, $h_{\mathrm{a}}=8$ m, $M=12$, $K=30$, and $\varepsilon=0.002$. Simulations are run in the MATLAB R2021b environment of an Intel Core i9-10900 CPU computer. We define the signal-to-noise ratio (SNR) as $\gamma_{\mathrm{sn}}=10\cdot\lg\left(\eta/\sigma_{\mathrm{n}}^2\right)$, where η is the average signal power and σ_{n}^2 is the noise power.

The first simulation considers a scenario with an ideal flat reflecting terrain. We compare the angle estimation performance of the BIML, 3D-BMLF, ARJE, beamspace RML (BRML), BJAI-not whitening (BJAI-NW), and BJAI-whitening (BJAI-W) algorithms against the Cramer–Rao bound (CRB) (Boman and Stoica, 2001). The conventional beamspace transformation matrix $\boldsymbol{T}_{\mathrm{B}}$ corresponds to the BJAI-NW algorithm, and the matrix $\boldsymbol{T}_{\mathrm{WB}}$, based on beamspace processing and whitening, corresponds to the BJAI-W algorithm. The proposed BJAI algorithm refers to the BJAI-W algorithm. We assume that $R_{\mathrm{d}}=100$ km, $H_{\mathrm{t}}=4500$ m, $\rho=0.9\mathrm{e}^{\mathrm{j}\pi}$, and the number of Monte Carlo trials is 1000.

First, we present a rough estimation of the target angle as shown in Fig. 2. Assuming that $M=12$ and $\gamma_{\mathrm{sn}}=10$ dB, by using the symmetry of the direct signal and the multipath signal, the estimated arrival angles of the target direct signal and multipath signal obtained through DBF scanning are relatively accurate. The measured value of the beam scanning is within half the beam width of the true values of the target direct

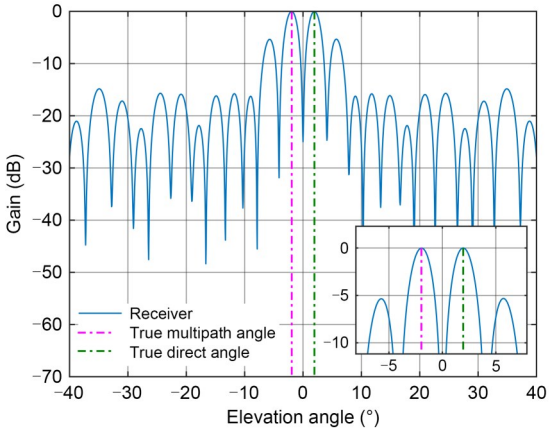

Fig. 2 Initial angle estimation by DBF scanning in simplified model. References to color refer to the online version of this figure

angle and multipath angle. This estimation provides a reasonable initial value and search interval for the subsequent algorithm iteration process.

Second, the change curves of the root mean square error (RMSE) for target elevation angle and height estimation by each algorithm with SNR are shown in Figs. 3 and 4, respectively, when the target is at an altitude of 4500 m. The figures show that the accuracy of angle and height estimation increases as the SNR increases. The estimation accuracies of the BIML, 3D-BMLF, and ARJE algorithms are relatively low due to their limited use of information. The BRML algorithm relies on prior information of the terrain. Under ideal flat terrain, it can obtain terrain-related parameters based on the determined geometric structure and has high angle estimation performance. The BJAI-NW algorithm relies mainly on $\boldsymbol{X}_{\mathrm{B}}$ for estimation, which is suboptimal when the noise of the beamspace data is not Gaussian white noise. On the other hand, the BJAI-W algorithm, which is based on the noise subspace and whitens the beamspace data, exhibits angle and height estimation accuracies that are relatively close to those of the CRB. This algorithm also enhances robustness and estimation accuracy by estimating the reflection coefficient $\bar{\rho}$ using additional information.

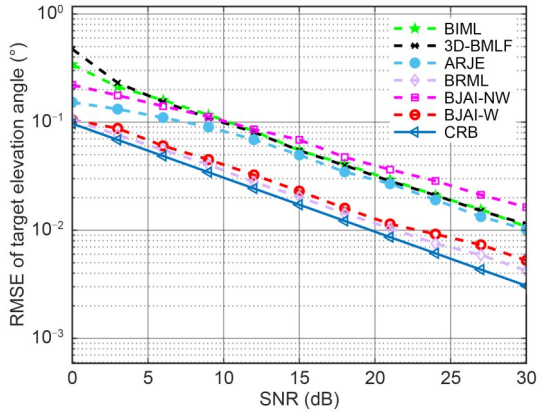

Fig. 3 RMSE of target elevation angle against SNR for H_{t}=4500 m

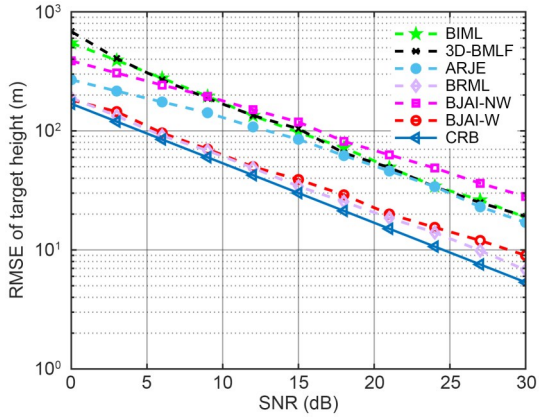

Fig. 4 RMSE of target height against SNR for H_{t}=4500 m

Finally, Table 1 shows the average running time of 200 Monte Carlo trials. The ARJE algorithm takes the most time because it is based on the element space, and the joint estimation and eigenvalue decomposition take up a lot of time. The 3D-BMLF algorithm completes angle estimation by finding a closed-form solution, so it takes the least time. The BIML algorithm can complete the target elevation angle estimation through a one-dimensional search. The BRML algorithm needs to calculate intermediate variables based on geometric structure and prior information, so the computational complexity is greater than that of the BIML algorithm. The BJAI-NW and BJAI-W algorithms complete angle estimation through joint alternating iterations, and the iterative processing brings additional computational complexity. Additionally, by converting the element space to the beamspace and using the initial estimation value to determine the angle search range, the computational complexity is reduced. In future research, we will explore low-complexity algorithms to make the proposed method more efficient.

Table 1 Running time comparison

Method	Running time (s)
BIML	0.0274
3D-BMLF	0.0017
ARJE	0.8164
BRML	0.0635
BJAI-NW	0.0497
BJAI-W	0.0525

The second simulation considers a complex scenario with undulating reflecting terrain. We assume that the target has a height of 9000 m, moving from 150 to 250 km in the horizontal direction. Due to the undulating terrain, we assume γ_{sn}=15 dB and $\rho=0.9\mathrm{e}^{\mathrm{j}\pi\cdot\Delta\gamma}$, where $\Delta\gamma$ represents the perturbation parameter, which reflects the degree to which the multipath signal is affected by the irregular reflection of the complex position and is an unknown variable. The form of

the perturbation parameter can be expressed as $\Delta\gamma=(1+\Delta\gamma_{\mathrm{a}})\mathrm{e}^{\mathrm{j}\pi\left(180°+\Delta\gamma_{\mathrm{p}}\right)/180°}$, where $\Delta\gamma_{\mathrm{a}}$ and $\Delta\gamma_{\mathrm{p}}$ represent the amplitude and phase perturbation of the perturbation parameter, respectively. We assume that the amplitude perturbation satisfies $\Delta\gamma_{\mathrm{a}}\sim U(-0.3,0.3)$ and that the phase perturbation satisfies $\Delta\gamma_{\mathrm{p}}\sim U(-30,30)$. A target point trace is generated every 10 km, and the target elevation angle corresponding to each point trace is estimated. The number of Monte Carlo trials is 1000.

Fig. 5 shows the angle estimation results of each point trace of the simulated target for each of the four beamspace algorithms, where the dotted line is the real elevation angle of the simulated target, and the point trace is the angle estimation result of the first 150 Monte Carlo tests. Fig. 6 shows the height estimation error for the simulated target. The BJAI-W algorithm has more accurate angle estimation results than other algorithms. When the target is far away and the elevation angle is low, affected by multipath perturbation, the BIML and 3D-BMLF algorithms cannot effectively distinguish between direct and multipath signals, and their performance is severely degraded. The BRML algorithm relies on prior information of the terrain. When the terrain is undulating and the terrain information is unknown, the BRML algorithm has a large angle estimation error, and the algorithm fails. Therefore, the algorithm proposed in this paper is suitable for dealing with low-elevation target height estimation problems under undulating terrain conditions.

By analyzing the proposed algorithm, we combine the reflection coefficient $\bar{\rho}$ and the target elevation angle θ_{d} for alternating iterative estimation. However, due to the complexity and variability of the actual surface environment, the positions of the multipath reflection points and the reflection coefficient change

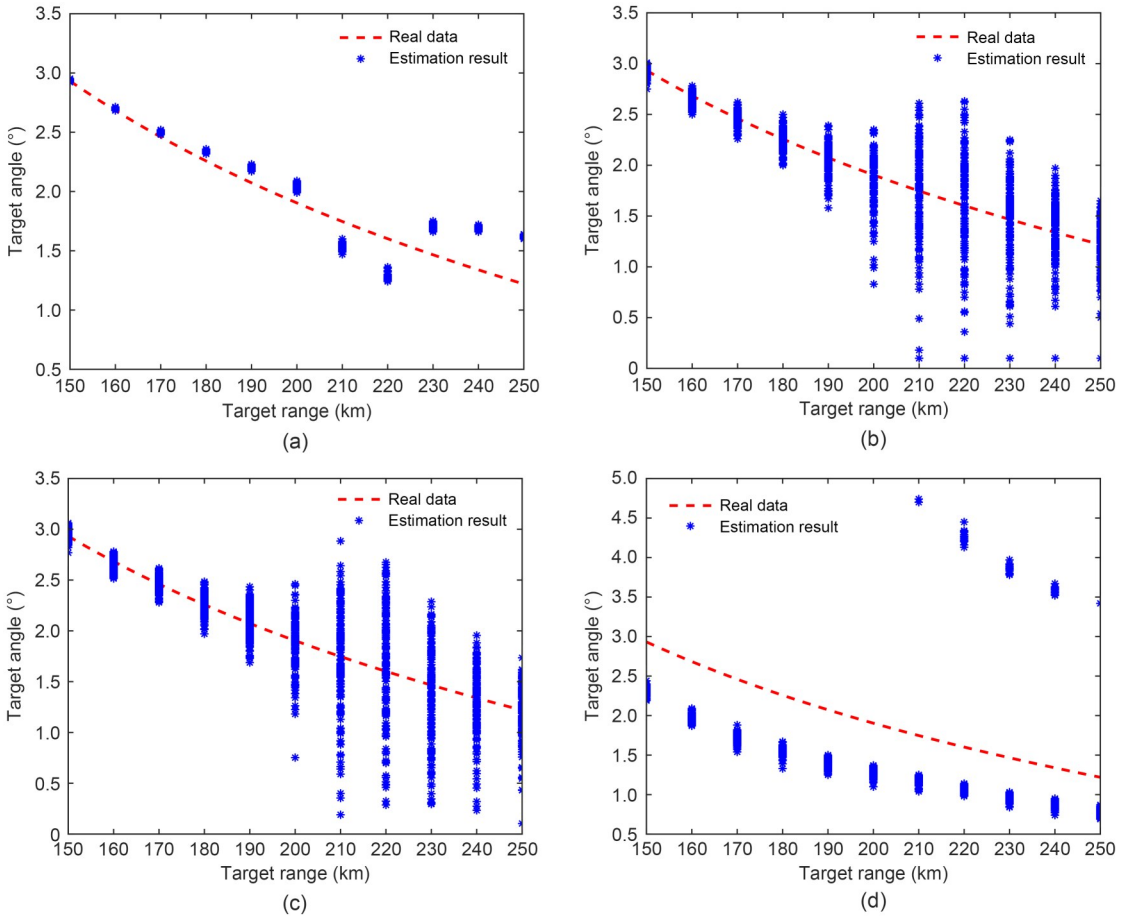

Fig. 5 Comparison of elevation angle estimation results for the simulated target of BJAI-W (a), BIML (b), 3D-BMLF (c), and BRML (d) algorithms

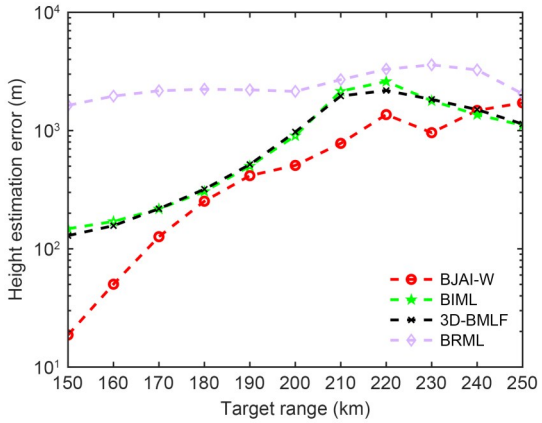

Fig. 6 Comparison of height estimation errors for the simulated target

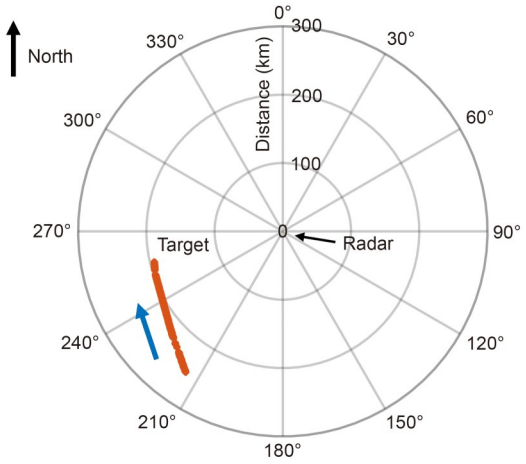

Fig. 7 Navigational trace map of the target. References to color refer to the online version of this figure

as the target moves. This can lead to degradation in the performance of existing algorithms that rely on deterministic scene geometry structure information and even failure in severe cases. Therefore, by using the information of the reflection coefficient $\bar{\rho}$, the proposed algorithm shows promising potential even under undulating terrain.

4.2 Real data validation

To further verify the performance of the proposed height estimation algorithm under complex terrain scenarios, real data are applied. The array radar is equipped with a uniform linear array and works in the meter band. The polarization mode is horizontal polarization. After the original data are processed by pulse compression, moving target indication (MTI), and constant false alarm detection, due to the limitation of the radar system, only one snapshot of measured data could be obtained for height estimation. Fig. 7 shows the flight trajectory of the target relative to the radar position, where the blue arrow indicates the flight direction. Fig. 8 shows the changes in the distance and azimuth of the target relative to the radar against frames. The radar is set up at the junction of land and sea, and the flight trajectory of the target is located over land, which includes irregular reflective surfaces such as undulating hills, fish ponds, and paddy fields.

Since the ARJE algorithm performs poorly under a single snapshot, we verify the proposed algorithm with the BIML and 3D-BMLF algorithms using real data. Figs. 9 and 10 show the processing results of the real data. The angle and height estimation performance

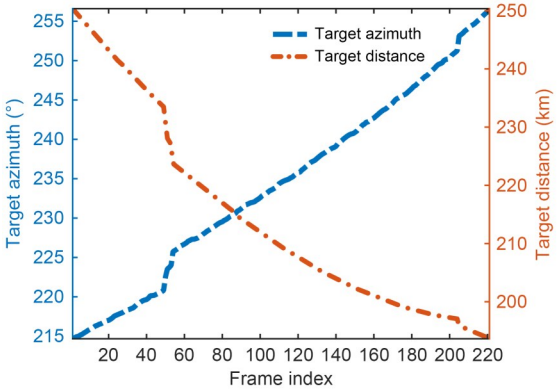

Fig. 8 Target azimuth and distance against frames

of the proposed algorithm is better than that of the other two algorithms. The estimation results of the 3D-BMLF algorithm have large errors, mainly because the algorithm uses a closed-form solution obtained under an accurate model. As the complexity of the terrain increases, the performance of the algorithm severely deteriorates. The BIML algorithm has a large estimation error when the target elevation angle is low because the target elevation angle and the multipath angle are within a beam width, and the angle difference is approximately 1/3 of the beam width at that time. In addition, for some frames, the estimation results of the three algorithms all jump, which is due to a low SNR or problems with the original data. The proposed algorithm uses covariance matrix estimation, so single-snapshot data and a low SNR will cause errors in the estimation of the reflection coefficient. In general, since the proposed algorithm takes

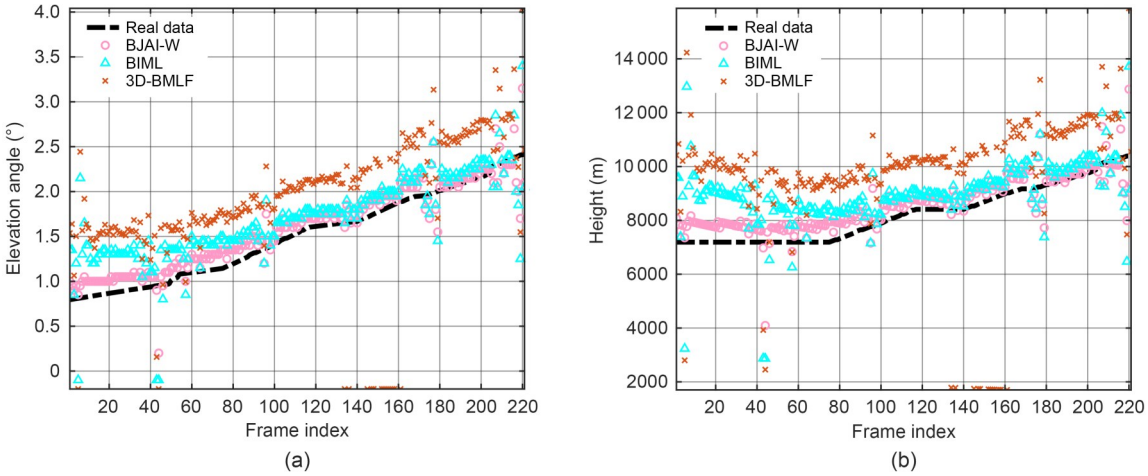

Fig. 9 Estimation results for real data: (a) target elevation angle; (b) target height

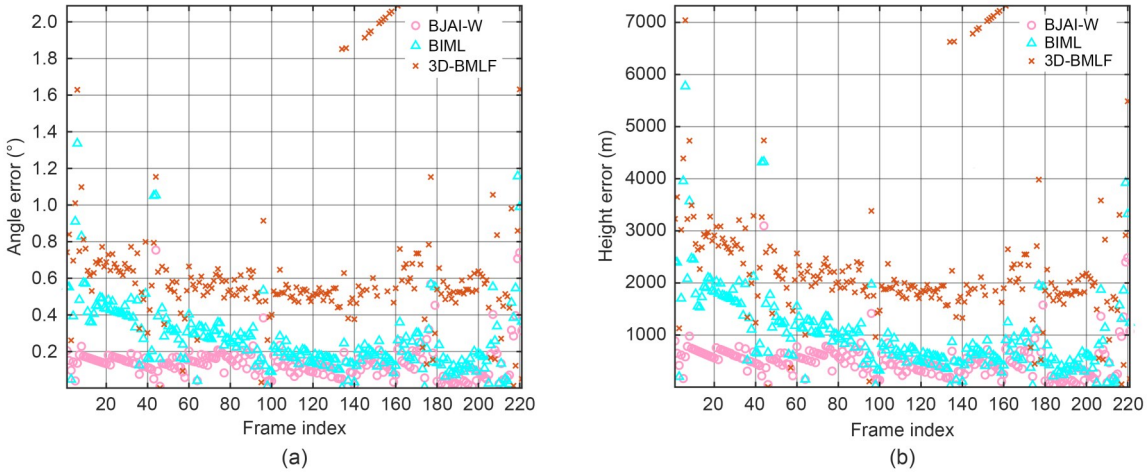

Fig. 10 Estimation error for real data: (a) elevation angle error; (b) height error

the effect of complex terrain into consideration and applies iterative estimation, it can resolve the reflection coefficient and target elevation angle. The effectiveness of the proposed algorithm is validated by experiment using real data.

5 Conclusions

We present a solution to the problem of estimating the target height for MIMO radar in a multipath environment. The proposed method, which is based on whitened beamspace data, achieves high estimation accuracy through the reflection coefficient and target elevation angle JAI estimation. The proposed algorithm improves the performance of target height estimation in complex multipath environments without any prior information about the reflected path. Numerical results based on simulated data and real data show the efficiency of our proposed algorithm under complex scenarios.

The multipath reflection coefficient model is dynamic. The model works well in simple undulating terrain scenarios but is difficult to match with the actual situation of more complex scenarios, which leads to the failure of the model. At present, it is difficult to build a model that can accurately match complex scenarios, but it is feasible to estimate the reflection coefficient. For more complex terrain conditions, we are now studying more matched multipath reflection models to improve the estimation performance for low-elevation targets.

Contributors

Derui TANG designed the research. Derui TANG and Yongbo ZHAO processed the data. Derui TANG drafted the paper. Shuaijie ZHANG helped organize the paper. Derui TANG and Yongbo ZHAO revised and finalized the paper.

Conflict of interest

All the authors declare that they have no conflict of interest.

Data availability

The data that support the findings of this study are available from the corresponding author upon reasonable request.

References

Boman K, Stoica P, 2001. Low angle estimation: models, methods, and bounds. *Dig Signal Process*, 11(1):35-79. https://doi.org/10.1006/dspr.2000.0373

Carlin M, Rocca P, Oliveri G, et al., 2013. Directions-of-arrival estimation through Bayesian compressive sensing strategies. *IEEE Trans Antenn Propag*, 61(7):3828-3838. https://doi.org/10.1109/TAP.2013.2256093

Chen C, Tao JF, Zheng GM, et al., 2022. Meter-wave MIMO radar height measurement method based on adaptive beamforming. *Dig Signal Process*, 120:103272. https://doi.org/10.1016/j.dsp.2021.103272

Chen S, Zhao YB, Hu YL, et al., 2022. A beamspace maximum likelihood algorithm for target height estimation for a bistatic MIMO radar. *Dig Signal Process*, 122:103330. https://doi.org/10.1016/j.dsp.2021.103330

Feng MY, Yang YX, Shu Q, et al., 2021. An improved ESPRIT-based algorithm for monostatic FDA-MIMO radar with linear or nonlinear frequency increments. *IEEE Commun Lett*, 25(7):2375-2379. https://doi.org/10.1109/LCOMM.2021.3075208

Gage KS, Green JL, 1978. Evidence for specular reflection from monostatic VHF radar observations of the stratosphere. *Radio Sci*, 13(6):991-1001. https://doi.org/10.1029/RS013i006p00991

Li J, Stoica P, 2007. MIMO radar with colocated antennas. *IEEE Signal Process Mag*, 24(5):106-114. https://doi.org/10.1109/MSP.2007.904812

Liu J, Liu Z, Xie R, 2010. Low angle estimation in MIMO radar. *Electron Lett*, 46(23):1565-1566. https://doi.org/10.1049/el.2010.2579

Liu J, Zhou WD, Juwono FH, et al., 2017. Reweighted smoothed L_0-norm based DOA estimation for MIMO radar. *Signal Process*, 137:44-51. https://doi.org/10.1016/j.sigpro.2017.01.034

Liu Y, Liu HW, Xia XG, et al., 2018. Projection techniques for altitude estimation over complex multipath condition-based VHF radar. *IEEE J Sel Top Appl Earth Obs Remote Sens*, 11(7):2362-2375. https://doi.org/10.1109/JSTARS.2018.2835448

Lo T, Litva J, 1991. Use of a highly deterministic multipath signal model in low-angle tracking. *IEE Proc F (Radar Signal Process)*, 138(2):163-171. https://doi.org/10.1049/ip-f-2.1991.0022

Shi JP, Hu GP, Zong BF, et al., 2016. DOA estimation using multipath echo power for MIMO radar in low-grazing angle. *IEEE Sens J*, 16(15):6087-6094. https://doi.org/10.1109/JSEN.2016.2580621

Shi JP, Wen FQ, Liu TP, 2021. Nested MIMO radar: coarrays, tensor modeling, and angle estimation. *IEEE Trans Aerosp Electron Syst*, 57(1):573-585. https://doi.org/10.1109/TAES.2020.3034012

Tan J, Nie ZP, 2018. Cramer–Rao bound of low angle estimation for VHF monostatic MIMO radar. Proc IEEE Radar Conf, p.158-163. https://doi.org/10.1109/RADAR.2018.8378549

Tang DR, Zhao YB, Niu B, et al., 2024. Bistatic MIMO radar height estimation method based on adaptive beamspace RML data fusion. *Dig Signal Process*, 145:104346. https://doi.org/10.1016/j.dsp.2023.104346

Wang SH, Cao YH, Su HT, et al., 2016. Target and reflecting surface height joint estimation in low-angle radar. *IET Radar Sonar Navig*, 10(3):617-623. https://doi.org/10.1049/iet-rsn.2015.0391

Wang XP, Wang W, Li X, et al., 2015. Real-valued covariance vector sparsity-inducing DOA estimation for monostatic MIMO radar. *Sensors*, 15(11):28271-28286. https://doi.org/10.3390/s151128271

Xu BQ, Zhao YB, 2019. Transmit beamspace-based DOD and DOA estimation method for bistatic MIMO radar. *Signal Process*, 157:88-96. https://doi.org/10.1016/j.sigpro.2018.11.016

Yang JY, Kang Y, Zhang Y, et al., 2020. A Bayesian angular superresolution method with lognormal constraint for sea-surface target. *IEEE Access*, 8:13419-13428. https://doi.org/10.1109/ACCESS.2020.2965973

Yin DY, Zhang F, 2020. Uniform linear array MIMO radar unitary root MUSIC angle estimation. Proc Chinese Automation Congress, p.578-581. https://doi.org/10.1109/CAC51589.2020.9327698

Zhang X, Huang Y, Chen C, et al., 2012. Reduced-complexity Capon for direction of arrival estimation in a monostatic multiple-input multiple-output radar. *IET Radar Sonar Navig*, 6(8):796-801. https://doi.org/10.1049/iet-rsn.2011.0343

Zheng GM, Song YW, Chen C, 2022. Height measurement with meter-wave polarimetric MIMO radar: signal model and MUSIC-like algorithm. *Signal Process*, 190:108344. https://doi.org/10.1016/j.sigpro.2021.108344

Zheng GM, Song YW, Liu YB, et al., 2023. Search-free range and angle estimation for bistatic VHF-FDA-MIMO radar in complex terrain. *Signal Process*, 212:109163. https://doi.org/10.1016/j.sigpro.2023.109163

Zhou WD, Liu J, Zhu PX, et al., 2016. Noncircular sources-based sparse representation algorithm for direction of arrival estimation in MIMO radar with mutual coupling. *Algorithms*, 9(3):61. https://doi.org/10.3390/a9030061

Zhu YT, Zhao YB, Shui PL, 2017. Low-angle target tracking

using frequency-agile refined maximum likelihood algorithm. *IET Radar Sonar Navig*, 11(3):491-497. https://doi.org/10.1049/iet-rsn.2016.0301

Ziskind I, Wax M, 1988. Maximum likelihood localization of multiple sources by alternating projection. *IEEE Trans Acoust Speech Signal Process*, 36(10):1553-1560. https://doi.org/10.1109/29.7543

Zoltowski MD, Lee TS, 1991. Maximum likelihood based sensor array signal processing in the beamspace domain for low angle radar tracking. *IEEE Trans Signal Process*, 39(3): 656-671. https://doi.org/10.1109/78.80885

Appendix: Proof of Claim 1

The columns of $\boldsymbol{E}_{\mathrm{s}}$ span the signal subspace, which coincides with the column space of $\boldsymbol{C}\left(\bar{\rho}, \hat{\theta}_{\mathrm{d}}^{(k)}\right)$, and the signal subspace is orthogonal to the noise subspace spanned by the columns of $\boldsymbol{E}_{\mathrm{n}}$. Therefore, we obtain

$$\left\| \boldsymbol{E}_{\mathrm{n}}^{\mathrm{H}} \boldsymbol{T}_{\mathrm{WB}} \boldsymbol{P} \cdot \boldsymbol{C}\left(\bar{\rho}, \hat{\theta}_{\mathrm{d}}^{(k)}\right) \right\|_2^2 = 0. \tag{A1}$$

For the $(k+1)^{\mathrm{th}}$ iteration, the algorithm begins with the obtained $\hat{\theta}_{\mathrm{d}}^{(k)}$ to find $\hat{\bar{\rho}}^{(k+1)}$ to minimize the cost function, which can be represented as

$$\begin{aligned}\hat{\bar{\rho}}^{(k+1)} = \arg\min_{\bar{\rho}} & \boldsymbol{C}^{\mathrm{H}}(\bar{\rho}, \hat{\theta}_{\mathrm{d}}^{(k)}) \boldsymbol{P}^{\mathrm{H}} \boldsymbol{T}_{\mathrm{WB}}^{\mathrm{H}} \boldsymbol{E}_{\mathrm{n}} \boldsymbol{E}_{\mathrm{n}}^{\mathrm{H}} \boldsymbol{T}_{\mathrm{WB}} \boldsymbol{P} \\ & \cdot \boldsymbol{C}(\bar{\rho}, \hat{\theta}_{\mathrm{d}}^{(k)}).\end{aligned} \tag{A2}$$

For convenience, we assume that $\boldsymbol{V}=\boldsymbol{T}_{\mathrm{WB}}\boldsymbol{P}$, $\boldsymbol{Q}=\left[c\left(\hat{\theta}_{\mathrm{d}}^{(k)}\right), c\left(\hat{\theta}_{\mathrm{m}}^{(k)}\right)\right]$, $\boldsymbol{\xi}=\left[1, \bar{\rho}\right]^{\mathrm{T}}$. Then, we can obtain

$$\hat{\bar{\rho}}^{(k+1)} = \arg\min_{\bar{\rho}} \boldsymbol{\xi}^{\mathrm{H}} \boldsymbol{Q}^{\mathrm{H}} \boldsymbol{V}^{\mathrm{H}} \boldsymbol{E}_{\mathrm{n}} \boldsymbol{E}_{\mathrm{n}}^{\mathrm{H}} \boldsymbol{V} \boldsymbol{Q} \boldsymbol{\xi}. \tag{A3}$$

This is an unconstrained optimization problem. Let $\boldsymbol{\omega}=\left[1, 0\right]^{\mathrm{T}}$. So the problem becomes an optimization problem under constraints:

$$\begin{aligned}&\min_{\bar{\rho}} \boldsymbol{\xi}^{\mathrm{H}} \boldsymbol{Q}^{\mathrm{H}} \boldsymbol{V}^{\mathrm{H}} \boldsymbol{E}_{\mathrm{n}} \boldsymbol{E}_{\mathrm{n}}^{\mathrm{H}} \boldsymbol{V} \boldsymbol{Q} \boldsymbol{\xi}, \\ &\text{s.t.} \quad \boldsymbol{\xi}^{\mathrm{H}} \boldsymbol{\omega} = 1.\end{aligned} \tag{A4}$$

The above problem can now be solved by the Lagrange multipliers. Let the objective function be

$$L(\boldsymbol{\xi}) = \boldsymbol{\xi}^{\mathrm{H}} \boldsymbol{Q}^{\mathrm{H}} \boldsymbol{V}^{\mathrm{H}} \boldsymbol{E}_{\mathrm{n}} \boldsymbol{E}_{\mathrm{n}}^{\mathrm{H}} \boldsymbol{V} \boldsymbol{Q} \boldsymbol{\xi} + \lambda (\boldsymbol{\xi}^{\mathrm{H}} \boldsymbol{\omega} - 1). \tag{A5}$$

Taking the partial derivatives of $\boldsymbol{\xi}$ and λ, we obtain

$$\begin{cases} \dfrac{\partial L}{\partial \boldsymbol{\xi}} = \boldsymbol{Q}^{\mathrm{H}} \boldsymbol{V}^{\mathrm{H}} \boldsymbol{E}_{\mathrm{n}} \boldsymbol{E}_{\mathrm{n}}^{\mathrm{H}} \boldsymbol{V} \boldsymbol{Q} \boldsymbol{\xi} + \lambda \boldsymbol{\omega} = \boldsymbol{0}, \\ \dfrac{\partial L}{\partial \lambda} = \boldsymbol{\xi}^{\mathrm{H}} \boldsymbol{\omega} - 1 = 0. \end{cases} \tag{A6}$$

Finally, we obtain

$$\boldsymbol{\xi} = \frac{[\boldsymbol{Q}^{\mathrm{H}} \boldsymbol{V}^{\mathrm{H}} \boldsymbol{E}_{\mathrm{n}} \boldsymbol{E}_{\mathrm{n}}^{\mathrm{H}} \boldsymbol{V} \boldsymbol{Q}]^{-1} \boldsymbol{\omega}}{\boldsymbol{\omega}^{\mathrm{H}} [\boldsymbol{Q}^{\mathrm{H}} \boldsymbol{V}^{\mathrm{H}} \boldsymbol{E}_{\mathrm{n}} \boldsymbol{E}_{\mathrm{n}}^{\mathrm{H}} \boldsymbol{V} \boldsymbol{Q}]^{-1} \boldsymbol{\omega}}. \tag{A7}$$